IEEE Access
Multidisciplinary | Rapid Review | Open Access Journal

Received August 10, 2019, accepted August 26, 2019, date of publication August 30, 2019, date of current version September 17, 2019.

Digital Object Identifier 10.1109/ACCESS.2019.2938681

A Robust Multi-Subject fMRI Analysis Method Using Dimensional Optimization

YAN ZHANG, MING LI, HUI SHEN, LING-LI ZENG, AND DEWEN HU, (Senior Member, IEEE)
College of Intelligence Science and Technology, National University of Defense Technology, Changsha 410073, China

Corresponding author: Ming Li (liming78@nudt.edu.cn)

This work was supported by the National Key Research and Development Program under Grant 2018YFB1305101.

ABSTRACT In blind source separation (BSS) for multisubject functional magnetic resonance imaging (fMRI) data, dimensionality reduction is generally performed for multiple times. This leads to the challenge of determining the number of the retained dimensionality, i.e. the order of BSS models, which dramatically influences the validity and performance of BSS models. In this study, a multisubject analysis method robust to order selection is developed. This approach remains effective for slight dimensionality reduction and thus utilizes more information from original data. Inspired by the idea of signal-intensity-maximization technology, which can suppress the overfitting that occurs during insufficient dimensionality reduction, we rotate the reduced dimensions to the optimized direction so that rotated components have the most significant intensity and smoothness. Because the optimized dimensions contain more useful information, involving dimensional optimization stage can reduce the negative impact of dimensionality reduction in multisubject data analysis. The experiments on simulated data and real fMRI data showed that involving dimensional optimization improves the validity and performance of the BSS model in analyzing multisubject data. The proposed method works better across a wide range of dimensionality reduction levels, allows inaccurate order selection, maintains more useful information, and is suitable for multisubject fMRI analysis, which requires multiple dimensionality reduction.

INDEX TERMS Blind source separation, functional magnetic resonance imaging, multisubject analysis, signal intensity maximization, dimensional optimization.

I. INTRODUCTION

Blind source separation (BSS) for functional magnetic resonance imaging (fMRI) data is an important topic in biomedical image analysis [1]–[3]. But when analyzing multi-set data, classical BSS methods meet the challenge of keeping the coherence among the estimated sources from multiple datasets [4].

Much effort has been made to achieve BSS for multisubject fMRI data. On one hand, some researchers reorganize data so that the multisubject data can be analyzed by classical BSS methods. For example, Calhoun *et al*. concatenated multiple datasets into a group prior to BSS, and proposed group independent component analysis (group ICA) [5]. On the other hand, some researchers extend classical BSS models so that multi-set data can be directly analyzed. Widely used methods in this scope include independent vector analysis (IVA) [6]–[8], multi-set canonical correlation analysis (M-CCA) [4], [9], [10], and generalized joint diagonalization (GJD) [11]–[13]. IVA extends the assumption of ICA from scalar values to source vectors, and attempts to maximize the independency across source vectors [14]. Lee *et al.* illustrated that the IVA model performs well in multisubject data analysis and does not require data concatenation [6]. Y.-O. Li *et al*. achieved joint BSS with M-CCA, an improved CCA model for multiple datasets, and demonstrated its better performance than IVA for sources with heterogeneous correlation values [4]. X.-L. Li *et al.* used GJD model to solve the problem of joint BSS, and demonstrated its superior performance compared to IVA and M-CCA for non-Gaussian sources [11].

Due to the high dimensionality of data, dimensionality reduction is generally performed two or more times before BSS approaches in multisubject fMRI data analysis. For example, in the group ICA procedure [5], both subject-level reduction on each subject's data and group-level reduction on the concatenated data of all subjects are performed. The number of retained dimensions is critical to the

The associate editor coordinating the review of this article and approving it for publication was Jeonghwan Gwak.

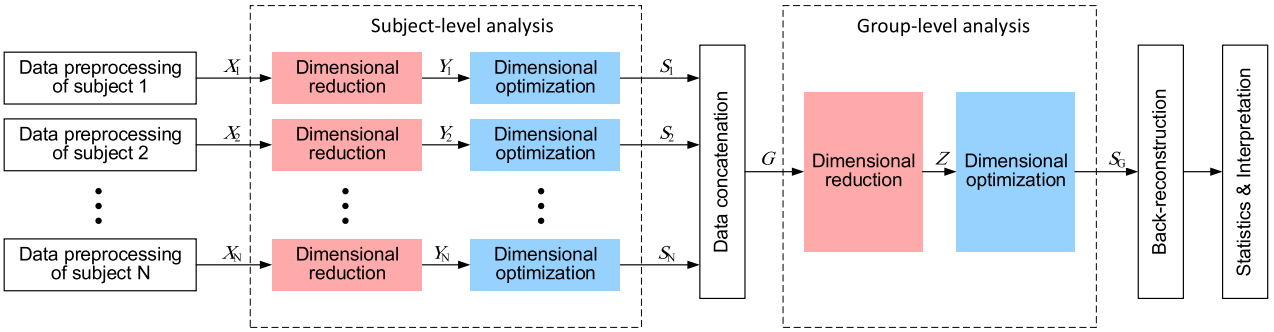

FIGURE 1. The procedure of the multi-subject data analysis involving dimension-optimization stage.

effectiveness of BSS models [2], [15]–[19], and multiple dimensional reductions will aggravate the sensitivity to model orders for multisubject analysis, therefore the retained dimensionality must be selected carefully for both subject-level and group-level reduction [1], [20]–[22]. If mismatch occurs between the determined number of retained dimensions and the real order, the BSS models may be invalid and yield unreliable results [23]–[25]. Although some criteria have been presented to evaluate the model order [26]–[30], accurately estimating the order is still challenging [31]. Furthermore, order estimation cannot reduce the risk of discarding interested dimensions because some useful signals may be so weak that they lie outside the remaining dimensions. Multiple dimensionality reductions in multisubject data analysis increase the risk of losing useful information.

In this study, to enhance the robustness of BSS models to the order number and reduce information loss, we attempted to improve the multisubject BSS algorithm by considering the idea of signal-intensity-maximization (SIM) technology [32]. A SIM-based dimensional optimization stage that helps to effectively utilize the retained dimensions after reduction is developed in this work. Because the SIM model is robust to the dimensionality reduction level and can work well even with high-dimensional data, by including the dimensional optimization stage, more dimensions can be retained during reduction in our algorithm, which allows more useful information to be utilized. A comparison using simulated data indicated that compared to the traditional algorithm, including dimensional optimization in multisubject analysis can improve the accuracy of the estimated spatial and temporal components. Our validation results on real fMRI data showed that the spatial and temporal components extracted by the proposed algorithm are more reasonable and interpretable. The involvement of dimensional optimization at both the subject and group levels during multisubject analysis achieved an outstanding and robust performance to order selection and was effective under insufficient dimensionality reduction.

II. METHOD AND MATERIALS

We illustrate the SIM-based dimensional optimization with the group analysis procedure proposed by Calhoun *et al.* [5]. Our procedure is shown in Fig. 1 and the dimensional optimization stage is applied after the subject-level and group-level dimensionality reductions. In the optimization stage, the retained dimensions are linearly combined using the SIM concept, in order to effectively utilize useful information and increase the robustness to the number of the retained dimensions.

A. SUBJECT-LEVEL DIMENSION-OPTIMIZATION

In the dimension-optimization stage, the SIM concept is applied to optimize the remained dimensions after data reduction so that the optimized components have the most significant intensity and smoothness. The signals after optimization (indicated by s_i for the i-th signal) should fulfill the maximal autocorrelation hypothesis (CCA hypothesis [2]) to distinguish meaningful signals and maintain sufficient signal intensity to retain useful information. The optimization problem is formulated as follows:

$$Obj = \theta \cdot \gamma_i + (1 - \theta) \cdot g_i, \tag{1}$$

where γ_i and g_i denote the autocorrelation and intensity of s_i, respectively, and θ is a real number within the interval (0,1). According to the CCA model [2], γ_i can be represented by the following formula:

$$\gamma_i = \frac{\mathrm{E}\left(s_i \left(s_i^{s(\Delta)}\right)^{\mathrm{T}}\right)}{\mathrm{E}\left(s_i^2\right)}, \tag{2}$$

where $s_i^{s(\Delta)}$ is the rotational shifted version of s_i, and the superscript $s(\Delta)$ denotes a shift of step Δ. Here, we develop the model under the condition in which the dimensionality reduction is performed by principal component analysis (PCA) at both subject and group levels. Assume that $X = (x_1, \ldots, x_n)^{\mathrm{T}}$ is the preprocessed data for a single subject. First, X is dimensionally reduced to $Y = (y_1, \ldots, y_{K1})^{\mathrm{T}}$ during the subject-level analysis, where y_i $(1 \le i \le K_1)$ is one of the K_1 $(K_1 \le n)$ retained principle components after the PCA processing and y_i has been normalized, i.e., $\mathrm{E}(y_i^2) = 1$.

According to PCA theory, $y_i = (\varphi_i)^{\mathrm{T}} X / |\lambda_i|$, where φ_i and λ_i^2 are the i-th eigenvector and eigenvalue of $\mathrm{E}(XX^{\mathrm{T}})$, respectively [33]. We then have

$$\begin{aligned} Y &= diag\left(1/|\lambda_1|, \ldots, 1/|\lambda_{K_1}|\right)\left(\varphi_1, \varphi_2, \ldots, \varphi_{K_1}\right)^{\mathrm{T}} X \\ &= \Lambda^{-1}\Phi^{\mathrm{T}} X \end{aligned} \tag{3}$$

where $\Lambda = diag(|\lambda_1|, |\lambda_2|, \ldots, |\lambda_{K1}|)$ and $\Phi = (\varphi_1, \varphi_2, \ldots, \varphi_{K1})$. The signals $s_1, \ldots, s_r$ are obtained from the dimension- optimization after the subject-level PCA analysis; therefore, s_i can be modeled as a linear combination of Y:

$$s_i = w_i^{\mathrm{T}} Y, \tag{4}$$

where w_i is the demixing vector corresponding to s_i, and $\|w_i\| = 1$.

The total intensity υ_i of s_i is determined by the following equation in SIM [32], which represents the significance of s_i:

$$\upsilon_i = \frac{\mathrm{E}^{\mathrm{T}}\left(Xs_i^{\mathrm{T}}\right)\mathrm{E}\left(Xs_i^{\mathrm{T}}\right)}{\mathrm{E}^2\left(s_i^2\right)}. \tag{5}$$

Inserting (3) and (4) into (5), the representation of the total signal intensity of the s_i can be reduced to

$$\begin{aligned}\upsilon_i &= \frac{\mathrm{E}^{\mathrm{T}}(XY^{\mathrm{T}}w_i)\mathrm{E}(XY^{\mathrm{T}}w_i)}{\mathrm{E}^2\left(w_i^{\mathrm{T}}YY^{\mathrm{T}}w_i\right)} \\ &= \frac{w_i^{\mathrm{T}}\mathrm{E}(YX^{\mathrm{T}})\mathrm{E}(XY^{\mathrm{T}})w_i}{\left(w_i^{\mathrm{T}}\mathrm{E}(YY^{\mathrm{T}})w_i\right)^2} \\ &= w_i^{\mathrm{T}}\Lambda^{-1}\Phi^{\mathrm{T}}\mathrm{E}\left(XX^{\mathrm{T}}\right)^2\Phi\Lambda^{-1}w_i \\ &= w_i^{\mathrm{T}}\Lambda^2 w_i. \end{aligned} \tag{6}$$

It is easy to obtain that the value of υ_i is in the interval $[0, \lambda_1^2]$. υ_i is then rescaled to the interval of [0,1] for normalization. Therefore the value of normalized υ_i becomes comparable to γ_i and it will be convenient to adjust their proportion by changing the value of θ. We now have the signal intensity term g_i:

$$g_i = \upsilon_i \Big/ \lambda_1^2 = w_i^{\mathrm{T}}\Lambda^2 w_i \Big/ \lambda_1^2. \tag{7}$$

Sequentially inserting (2), (4), and (7) into (1), we then obtain the expression of the objective function:

$$\begin{aligned} Obj &= w_i^{\mathrm{T}}\left(\theta \cdot \mathrm{E}\left(Y\left(Y^{s(\Delta)}\right)^{\mathrm{T}}\right) + (1-\theta)\cdot\Lambda^2\Big/\lambda_1^2\right)w_i \\ &= w_i^{\mathrm{T}}Uw_i, \end{aligned} \tag{8}$$

where $U = \theta \cdot \mathrm{E}(Y(Y^{s(\Delta)})^{\mathrm{T}}) + (1-\theta)\cdot\Lambda^2/\lambda_1^2$.

Under the constraint $\|w_i\| = 1$, the w_i values cause Obj to approach its extrema are the eigenvectors of $U + U^{\mathrm{T}}$. The demixing matrix W for all signals after optimization consists of the eigenvectors of $U + U^{\mathrm{T}}$, i.e., $W = (w_1, \ldots, w_r)$.

Based on the demixing matrix W and the subject-level dimensionally reduced data Y, the component map $S = (s_1, \ldots, s_r)^{\mathrm{T}}$ after dimensional optimization can be obtained by

$$S = W^{\mathrm{T}}Y. \tag{9}$$

B. GROUP-LEVEL DIMENSION-OPTIMIZATION

Similar to subject-level dimension-optimization, we can obtain the objective function Obj and autocorrelation term γ_i represented by (1) and (2) respectively. Here, we use X_m to represent the preprocessed data matrix from the m-th subject to replace X in the previous subsection. In contrast to (5), for each subject, we can obtain the total intensity of an optimized signal $s_{G,i}$, termed $\upsilon_{m,i}$ for the m-th subject. Then, $\upsilon_{m,i}$ will be written as:

$$\upsilon_{m,i} = \frac{\mathrm{E}^{\mathrm{T}}(X_m s_{G,i}^{\mathrm{T}})\mathrm{E}(X_m s_{G,i}^{\mathrm{T}})}{\mathrm{E}^2(s_{G,i}^2)}. \tag{10}$$

After subject-level analysis for all subjects, the data are then concatenated into a data matrix G for group-level analysis and dimensionally reduced to $Z = (z_1, \ldots, z_{K2})^{\mathrm{T}}$, where $z_i (1 \le i \le K_2)$ is one of the K_2 ($K_2 \le K_1$ and K_2 is generally set equal to K_1) retained principle components after PCA and z_i has been normalized, i.e., $\mathrm{E}(z_i^2) = 1$. According to the theory of PCA, $z_i = \psi_i^{\mathrm{T}}G/|\mu_i|$, where ψ_i and μ_i^2 are the i-th eigenvector and eigenvalue of $\mathrm{E}(GG^{\mathrm{T}})$, respectively. We then have

$$\begin{aligned} Z &= diag\left(1/|\mu_1|, \ldots, 1/|\mu_{K_2}|\right)\left(\psi_1, \ldots, \psi_{K_2}\right)^{\mathrm{T}} G \\ &= \Lambda_G^{-1}\Psi^{\mathrm{T}}G, \end{aligned} \tag{11}$$

where $\Lambda_G = diag(|\mu_1|, |\mu_2|, \ldots, |\mu_{K2}|)$ and $\Psi = (\psi_1, \psi_2, \ldots, \psi_{K2})$. Similar to (4), the demixing model can be written as $S_G = W_G^{\mathrm{T}}Z$, where $S_G = (s_{G,1}, \ldots s_{G,r})^{\mathrm{T}}$ is the signal map after group-level dimension-optimization and $W_G = (w_{G,1}, \ldots w_{G,r})$ is the demixing matrix. Thus, we obtain

$$s_{G,i} = w_{G,i}^{\mathrm{T}}Z. \tag{12}$$

Inserting (12) into (10), the representation of the total intensity of $s_{G,i}$ for the m-th subject can be reduced to

$$\begin{aligned}\upsilon_{m,i} &= \frac{\mathrm{E}^{\mathrm{T}}(X_m Z^{\mathrm{T}}w_{G,i})\mathrm{E}(X_m Z^{\mathrm{T}}w_{G,i})}{\mathrm{E}^2(w_{G,i}^{\mathrm{T}}ZZ^{\mathrm{T}}w_{G,i})} \\ &= \frac{w_{G,i}^{\mathrm{T}}\mathrm{E}(ZX_m^{\mathrm{T}})\mathrm{E}(X_m Z^{\mathrm{T}})w_{G,i}}{(w_{G,i}^{\mathrm{T}}\mathrm{E}(ZZ^{\mathrm{T}})w_{G,i})^2} \\ &= w_{G,i}^{\mathrm{T}}\mathrm{E}(ZX_m^{\mathrm{T}})\mathrm{E}(X_m Z^{\mathrm{T}})w_{G,i}. \end{aligned} \tag{13}$$

Then, we can define the total intensity υ_i of $s_{G,i}$ for all subjects as follows:

$$\begin{aligned}\upsilon_i &= \sum_m \upsilon_{m,i} \\ &= \sum_m w_{G,i}^{\mathrm{T}}\mathrm{E}(ZX_m^{\mathrm{T}})\mathrm{E}(X_m Z^{\mathrm{T}})w_{G,i} \\ &= w_{G,i}^{\mathrm{T}}\cdot\sum_m \mathrm{E}(ZX_m^{\mathrm{T}})\mathrm{E}(X_m Z^{\mathrm{T}})\cdot w_{G,i}. \end{aligned} \tag{14}$$

Assuming that there are N subjects in total, it is easy to find that the value of $\mathrm{E}(ZX_m^{\mathrm{T}})\mathrm{E}(X_m Z^{\mathrm{T}})$ lies in the interval $[0, N\lambda_{m,1}^2]$, where $\lambda_{m,1}^2$ is the first eigenvalue of $\mathrm{E}(X_m X_m^{\mathrm{T}})$.

Then, υ_i is normalized to the interval [0,1]. We now have the intensity-term g_i:

$$g_i = w_{G,i}^{\mathrm{T}} \cdot \sum_m \frac{\mathrm{E}(ZX_m^{\mathrm{T}})\mathrm{E}(X_m Z^{\mathrm{T}})}{N\lambda_{m,1}^2} \cdot w_{G,i}. \tag{15}$$

Sequentially inserting (2), (12), and (15) into (1), we can obtain the expression of the objective function:

$$\begin{aligned} Obj &= w_{G,i}^{\mathrm{T}} \left(\theta \cdot \mathrm{E}\left(Z \left(Z^{s(\Delta)} \right)^{\mathrm{T}} \right) + (1-\theta) \right. \\ &\quad \left. \cdot \sum_m \left(\mathrm{E}(ZX_m^{\mathrm{T}})\mathrm{E}(X_m Z^{\mathrm{T}}) \Big/ N\lambda_{m,1}^2 \right) \right) w_{G,i} \\ &= w_{G,i}^{\mathrm{T}} U_G w_{G,i}, \end{aligned} \tag{16}$$

where

$$\begin{aligned} U_G = \theta \cdot \mathrm{E}(Z(Z^{s(\Delta)})^{\mathrm{T}}) + (1-\theta) \\ \cdot \sum_m \frac{\mathrm{E}(ZX_m^{\mathrm{T}})\mathrm{E}(X_m Z^{\mathrm{T}})}{N\lambda_{m,1}^2}. \end{aligned} \tag{17}$$

Under the constraint $\|w_{G,i}\| = 1$, the $w_{G,i}$ values that cause Obj to approach its extrema are the eigenvectors of $U_G + U_G^{\mathrm{T}}$. The demixing matrix $W_G W$ for all the signals after dimension-optimization consists of the eigenvectors of $U_G + U_G^{\mathrm{T}}$, i.e., $W_G = (w_{G,1}, \ldots, w_{G,r})$.

According to the demixing matrix W_G and the group-level dimensionally reduced data Z, S_G can be obtained by

$$S_G = W_G^{\mathrm{T}} Z. \tag{18}$$

Sequentially inserting (3), (9), and (11) into (18), the component map of each subject can be back-reconstructed by

$$s_{G,i} = W_G^T \Lambda_G^{-1} \Psi^{\mathrm{T}} W_i^{\mathrm{T}} Y_i, \tag{19}$$

where the matrix $s_{G,i}$ contains the single subject maps for subject i and $W_G^T \Lambda_G^{-1} \Psi^{\mathrm{T}} W_i^{\mathrm{T}}$ is the mixing matrix for Y_i.

C. DATASET AND PREPROCESSING

Two datasets were used to validate the proposed method by comparisons with other multisubject analysis methods. The first dataset consists of resting-state fMRI data and was employed as the background when generating simulated data. The second dataset is task fMRI data and was used to compare with the group ICA method on real fMRI data.

Dataset 1: Resting-state fMRI data from ten young and healthy subjects were collected on a 1.5T Philips Intera MR scanner at the Second Xiangya Hospital of Central South University [34], [35]. All the subjects provided written informed consent after receiving a complete description of the study. Functional images were acquired using a gradient-echo echo-planar pulse sequence over a 6-min period for a total of 180 time points with the following parameters: TR = 2 s, TE = 30 ms, thickness/gap = 4.5 / 0 mm, field of view (FOV) = 230 × 230 mm, flip angle (FA) = 90°, matrix = 128 × 128, and 31 slices. This rsfMRI data were preprocessed using a statistical parametric mapping software package (SPM8, http://www.fil.ion.ucl.ac.uk/spm) [31], [36] and details of preprocessing steps are referred to [34].

Dataset 2: The second dataset was acquired from the publicly available Human Connectome Project (HCP) motor task fMRI data. The fMRI scans included ten movement blocks and three fixation blocks. In each task block, eight participants (in S500 release) were presented with visual cues that prompted them to perform certain movements to map motor areas; the movements included tapping their right or left fingers, squeezing their right or left toes, or moving their tongue. The tfMRI images were obtained by a modified Siemens Skyra 3 T scanner with a 32-channel head coil using the following acquisition parameters: 90 × 104 matrix, 220 mm FOV, TR = 720 ms, TE = 33.1 ms, flip angle = 52°, 72 slices, BW = 2290 Hz/Px, in-plane FOV = 208 × 180 mm, and 2.0 mm isotropic voxels. For the tfMRI data, the preprocessing pipeline included the removal of spatial artifacts and distortion, cortical surface generation, within-subject cross-modal registration, cross-subject registration to the MNI standard volume and surface spaces, resampling into 2.0 mm isotropic voxels and spatial smoothing. More detailed task descriptions and data preprocessing could be found in the literatures [37]–[39].

III. EXPERIMENTS

To test the validity of the proposed multisubject analysis approach involving dimensional optimization, we conducted a series of comparisons between the proposed approach and other multisubject analysis algorithms on both simulated and real fMRI data.

A. COMPARISON ON SIMULATED DATA

To evaluate and validate the proposed method, comparisons were first performed on simulated data generated by inserting simulated activation patterns into real resting-state fMRI data (Dataset 1) (see Fig. 2). The simulated activation pattern is composed of two 20 × 20 × 20 regions, and can be located in 300 different positions (Fig. 2(a)). The corresponding hemodynamic time course containing 175 time points was generated based on the time-course length of the resting-state fMRI images (Fig. 2(b)).

The first two experiments were designed for ablation study to explore the role of dimensional optimization at subject level and group level. Three simplified procedures (involving only subject-level optimization, involving only group-level optimization and involving no dimensional optimization) were conducted and compared with our method (involving both-level optimization).

In the first experiment, the study was achieved under various signal-to-noise ratio (SNR) conditions. The SNR was defined as the ratio between the standard deviation of the simulated source and the background. By changing the amplitude of the embedded simulated source, four SNR values ranging from 0.20 to 0.35 at a step size of 0.05 were set. For each SNR value, simulated data for ten subjects were generated to perform group analysis. After estimating each

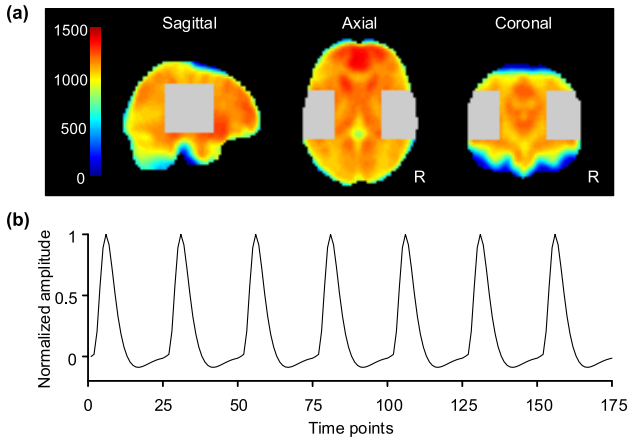

FIGURE 2. Generating the simulated data. A simulated "source" is embedded into the resting-state fMRI data. (a) The spatial view of the simulated data. The gray area is an example of the simulated activation pattern. (b) The simulated hemodynamic time course.

simulated dataset by the minimum description length (MDL) criterion [40], [41], the numbers of remained dimensions in subject-level and group-level dimensionality reduction were set to 15. We performed the proposed algorithm and group ICA on simulated data to obtain the group spatial maps, and group ICA was performed via GIFT toolbox (http://mialab.mrn.org/software/gift/index.html).

In the second experiment, the four procedures were compared across different dimensionality reduction levels to assess the robustness of different methods. The numbers of principal components retained by PCA were set to 10, 20, 40, 60, 80 and 100. The proposed algorithm and group ICA were then executed on the simulated data to obtain the group components. The SNR of the simulated data was set to 0.2 for the study on the difference of the robustness between the four procedures.

The third experiment was designed to compare the proposed method with recently developed multisubject analysis methods, including IVA [6], M-CCA [4] and GJD [11]. The remaining dimensions and SNR values are set to be identical to those in the first experiment.

B. COMPARISON ON fMRI DATA

This experiment was designed to evaluate and validate the proposed algorithm by comparing it with group ICA method on real fMRI data. The preprocessed HCP tfMRI data were analyzed by both the proposed method and the group ICA method, and the number of retained components was set to 20 using the minimum description length criterion, the details are similar to the number selection in simulated data. The group components were obtained by performing a one-sample t-test.

IV. RESULTS AND DISCUSSION

A. COMPARISON ON SIMULATED DATA

On the simulated data, to evaluate the role of dimensional optimization, our method was firstly compared with three

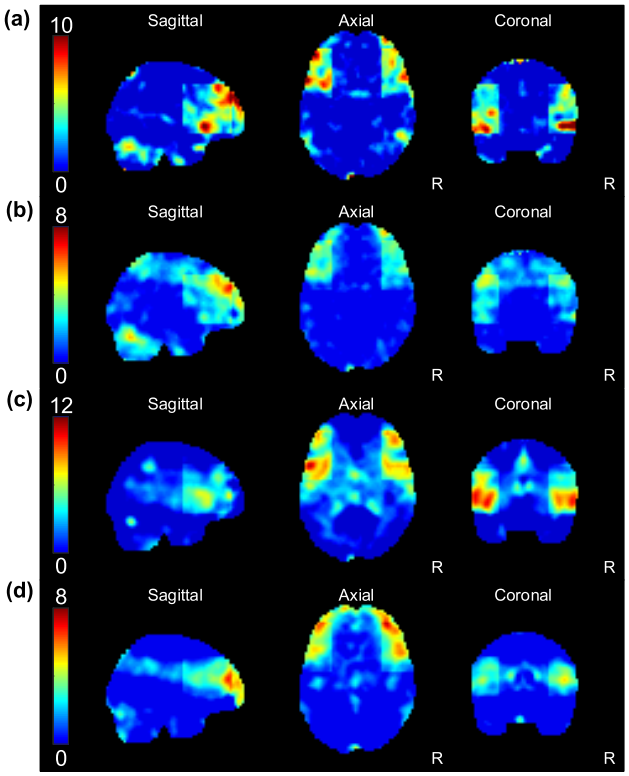

FIGURE 3. The spatial maps of group components obtained from a simulated dataset by four procedures: (a) involving dimensional optimization at both subject and group levels, (b) involving dimensional optimization only at subject level, (c) involving dimensional optimization only at group level, and (d) involving no dimensional optimization.

simplified procedures (removing dimensional optimization at different levels). Among the group components separated by each algorithm, the source that had the highest correlation with the simulated source was selected as the output of the algorithm (see the spatial maps in Fig. 3 as examples). Then, we plotted the receiver operating characteristic (ROC) curves [42] for the activated region determined by each algorithm. The area under the ROC curve (AUC) was used to evaluate each method. A larger AUC indicates that the determined activated region is more accurate and that the corresponding method achieves better performance [43]. To validate the effectiveness of the dimensional optimization in detecting the activated regions, the algorithms that only involve dimensional optimization once (at the subject level or group level individually) were also considered in this comparison.

Fig. 4 shows a comparison of the average AUC values of the four procedures when detecting the simulated activated region under various SNR conditions. At all SNRs, all three of our procedures achieve higher AUC values than the traditional multisubject analysis method, demonstrating that considering dimension-optimization increases the accuracy of activated-region detection.

Additionally, between the two algorithms involving single-level dimensional optimization (red and green bars), the red bars are considerably taller than the green bars. And the

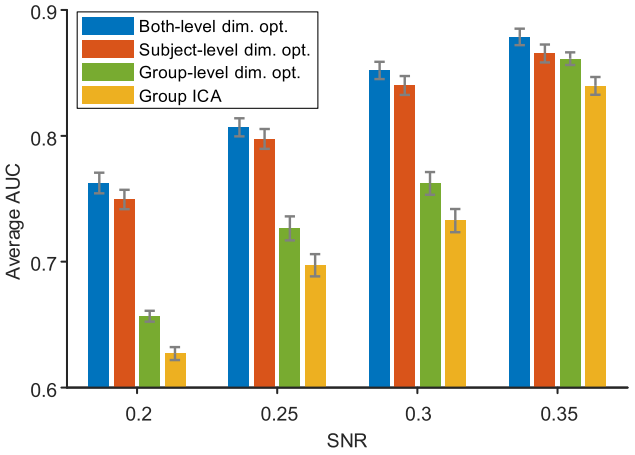

FIGURE 4. Comparison between our methods involving dimension-optimization and the conventional algorithm (group ICA) at various SNRs. The vertical axis indicates average AUC values, and the horizontal axis indicates SNR values. Yellow bars: Group ICA; Green bars: Involving dimension-optimization only at group level; Red bars: Involving dimension-optimization only at subject level; Blue bars: Involving dimension-optimization at both levels. The error bars show ± SEM.

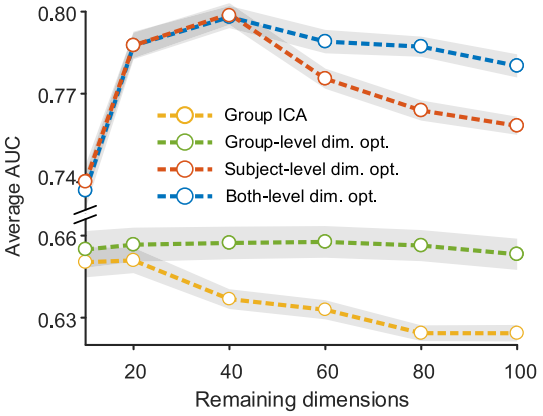

FIGURE 5. Performance comparison between our algorithms involving dimensional optimization and group ICA across different dimensionality reduction levels. The vertical axis indicates the average AUC values, and the horizontal axis indicates the number of remaining dimensions after dimensionality reduction. Yellow: Group ICA; Green: Involving dimension-optimization only at group level, Red: Involving dimension-optimization only at subject level; Blue: Involving dimension-optimization at both levels. The shadings represent ± SEM.

red bars are quite similar to the blue bars, which include optimization twice. In contrast, the green ones are much shorter and similar to the yellow bars, which do not involve dimensional optimization. This implies that dimensional optimization is more effective at the subject level than at the group level—possibly because it is more critical to retain the subject-level useful information, which is more easily lost during the dimensionality reduction. Because the SIM model helps to retain the most useful dimensions, the subject-level dimensional optimization retains much of the critical useful information from each subject and improves the performance of the algorithm. In contrast, because it loses many useful dimensions during the subject-level reduction, the algorithm with only group-level dimensional optimization achieves only limited performance.

It should be noted that, although slight, the group-level dimensional optimization also contributes to the improved performance of the algorithm. With the group-level dimensional optimization, the green bars are higher than the yellow bars, while without group-level dimensional optimization, the red bars are slightly shorter than the blue bars.

Fig. 5 shows the performance of the four procedures when the dimensionality reduction levels are varied. In Fig. 5, group ICA becomes worse as the dimensionality increases, suggesting that the validity of the ICA model is affected at high dimensions. In contrast, the three SIM-based algorithms perform better than the conventional method at all dimensionality reduction levels and are more robust to the dimensionality when the reduction is slight.

Note that the blue and red curves, both of which involve subject-level dimensional optimization, ascend sharply from 10 to 40 dimensions. This implies that much useful information still exists in these dimensions; thus, involving subject-level dimensional optimization can utilize that information to achieve a higher accuracy. In contrast, the green and yellow curves do not show better performance at a dimensionality of 40 than at a dimensionality of 10, suggesting that the useful information in the dimensions from 10^{th} to 40^{th} cannot be acquired without the subject-level dimensional optimization.

It should also be noted that the red curve, without group-level dimensional optimization, descends significantly when the remaining dimensions exceed 40, as does the conventional method, which also includes no group-level dimensional optimization. On the other hand, the green curve, with group-level dimensional optimization, shows strong robustness to the dimensionality retained. This implies that group-level dimensional optimization can improve the robustness of the method.

Nevertheless, the three algorithms involving dimensional optimization (the blue, red and green curves) maintain higher accuracy than the conventional algorithm, especially at high dimensions. The result suggests that involving dimensional optimization can improve the accuracy of the method (just as illustrated in Fig. 4), while the robustness is mainly improved by group-level dimensional optimization.

The main computational load of dimension-optimization, at either group level or subject level, is to solve the eigenvector of the covariance matrix, with a complexity of $O(d^3)$ (d is the number of remaining dimensions). Therefore, involving optimization at single level and at both level have the same asymptotic complexity.

Although the group-level optimization does not increase AUC values greatly, it can significantly increase the robustness to dimensionality reduction levels (Fig. 5). Considering the same asymptotic complexity, involving both-level optimization is recommended.

We further compared our method with other multisubject analysis methods at four different SNRs. Fig. 6 shows the comparison results between our method and other multisubject analysis methods. The spatial correlation was used as an

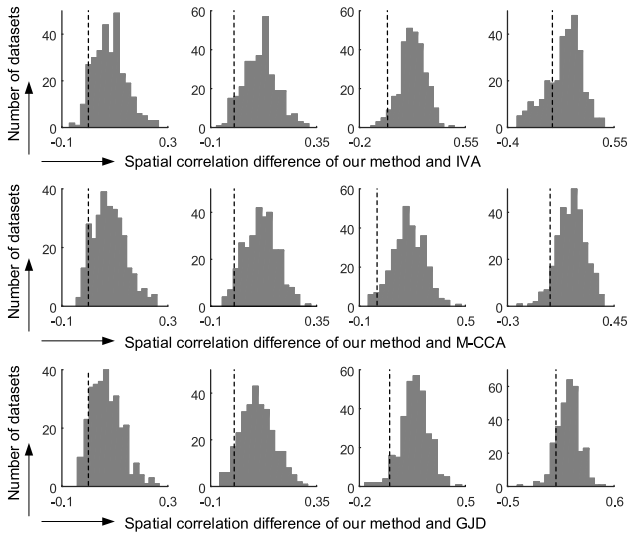

FIGURE 6. Performance comparison between our algorithm and other multisubject analysis methods. Each panel shows the histogram of the correlation difference values between our method and other methods. Positive values mean the spatial correlations of our method are larger than those of other methods. The zero of horizontal axis is marked by dashed line. First column: Results on SNR = 0.2, second column: SNR = 0.25, third column: SNR = 0.3, and fourth column: SNR = 0.35; first row: Comparison of our method and IVA, second row: Comparison of our method and M-CCA, and third row: Comparison of our method and GJD. At all SNRs, most of the difference values are positive, indicating that our method achieves higher spatial correlations than other methods on most of the datasets. This finding implies that our method achieved higher accuracy at all SNRs.

index to evaluate the group components obtained by different methods [7], [44]. Each histogram in Fig. 6 displays the correlation difference between our method and other methods on 300 datasets at each SNR. Positive difference values mean that the spatial correlations of our method are higher than those of other methods. From Fig. 6, it can be seen that most of the difference values are positive, indicating that our method achieves higher spatial correlations at most datasets. This result implies that our method achieves higher accuracy under all SNRs.

B. COMPARISON ON fMRI DATA

When analyzing the real fMRI data using our proposed method and group ICA, we selected two pairs of task-related components according to the spatial overlap and temporal correspondence. The spatial components and time courses of the group are presented in Figs. 7 and 8.

For each task-related component, we compared the spatial maps extracted by the two methods. Although they largely overlap, the activated regions obtained by the two methods show some clear differences (Fig. 7a–b, Fig. 8a–b). To examine the validity of the difference region (rest of regions in each component except overlap), we computed the correlations between the average time courses from the overlapped and difference regions for each subject, as shown in Table 1. Because the overlap can be considered as reliable activated regions, larger correlations to the overlapped region mean the difference region is more reasonable. From Table 1, we can

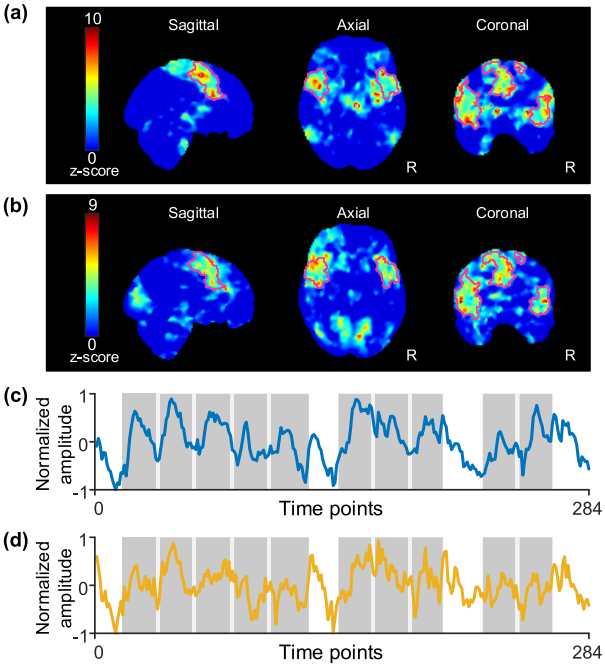

FIGURE 7. Spatial maps and time courses of the first task-related component derived from experiments on the task fMRI data by our method (a and c) and group ICA (b and d). The shadings represent the task contrast designs of the tfMRI data. The pink contours represent the overlapped regions of the two methods.

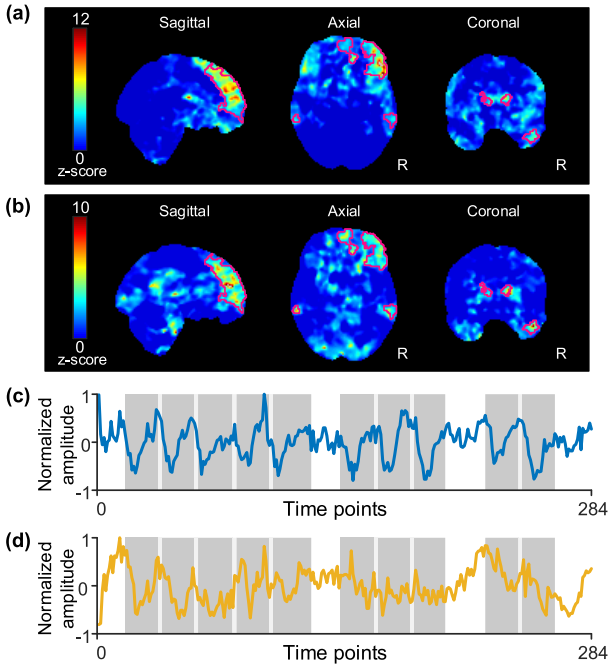

FIGURE 8. Spatial maps and time courses of the second task-related component derived from experiments on the task fMRI data by our method (a and c) and group ICA (b and d). The shadings represent the task contrast designs of the tfMRI data. The pink contours represent the overlapped regions of the two methods.

see that the correlations within each subject are all larger for both components when using our method (mean ± SD: 0.73 ± 0.09, 0.63 ± 0.11) than when using group ICA (mean ± SD: 0.24 ± 0.12, 0.13 ± 0.21), indicating that the spatial

TABLE 1. Correlations of The time courses between the overlapped region and difference region within each subject.

		Sub. 1	Sub. 2	Sub. 3	Sub. 4	Sub. 5	Sub. 6	Sub. 7	Sub. 8	Mean ± SD
Comp. #1	Our method	0.81	0.63	0.62	0.67	0.67	0.80	0.82	0.83	0.73 ± 0.09
	Group ICA	0.09	0.08	0.23	0.39	0.21	0.25	0.39	0.24	0.24 ± 0.12
Comp. #2	Our method	0.51	0.61	0.70	0.56	0.53	0.84	0.67	0.64	0.63 ± 0.11
	Group ICA	0.20	-0.05	0.20	0.30	0.26	0.41	-0.23	-0.02	0.13 ± 0.21

TABLE 2. Number of subjects showed difference between tasks and baseline.

	Comp. #1		Comp. #2	
	Our method	Group ICA	Our method	Group ICA
Task 1	6(75%)	4(50%)	6(75%)	4(50%)
Task 2	8(100%)	7(87.5%)	7(87.5%)	6(75%)
Task 3	6(75%)	3(37.5%)	6(75%)	4(50%)
Task 4	8(100%)	8(100%)	8(100%)	7(87.5%)
Task 5	8(100%)	8(100%)	8(100%)	6(75%)

components obtained by the proposed method are more reasonable.

To estimate the validity of the extracted temporal response, we examined whether each task can be significantly detected on the back-reconstructed time course of each subject. Within each back-reconstructed time course, we compared the BOLD level during task and fixation blocks and determined whether a significant difference exists between the task block and baseline (two-sample t-test, $\alpha = 0.05$). If the component is task-related, the difference should be significant for all subjects. Table 2 provides the number of subjects for which the difference is significant. As shown in the table, for both pairs of components, the percentage our method achieves when detecting significant differences is higher on every task and every subject. The results indicate that the time courses obtained by the proposed method both correspond better with the task paradigm and are easier to interpret.

V. CONCLUSION

The main goal of this study was to improve the multisubject data analysis algorithm with a SIM-based dimension-optimization stage which effectively helps utilize the useful dimensions after reduction. The comparisons show that inserting dimensional optimization—notably, at both subject and group levels—provides overall improvements in the accuracy and validity of detecting interested components and enhances the robustness of the method to model order. In comparison with other multisubject analysis methods, our SIM-based method, which involves dimensional optimization at both the subject and group levels, achieves higher accuracy under different noise conditions.

REFERENCES

[1] H. Li, N. M. Correa, P. A. Rodriguez, V. D. Calhoun, and T. Adali, "Application of independent component analysis with adaptive density model to complex-valued fMRI data," *IEEE Trans. Biomed. Eng.*, vol. 58, no. 10, pp. 2794–2803, Oct. 2011.

[2] O. Friman, M. Borga, P. Lundberg, and H. Knutsson, "Exploratory fMRI analysis by autocorrelation maximization," *NeuroImage*, vol. 16, no. 2, pp. 454–464, 2002.

[3] M. Li, Y. Liu, G. Feng, Z. Zhou, and D. Hu, "OI and fMRI signal separation using both temporal and spatial autocorrelations," *IEEE Trans. Biomed. Eng.*, vol. 57, no. 8, pp. 1917–1926, Aug. 2010.

[4] Y.-O. Li, T. Adalı, W. Wang, and V. D. Calhoun, "Joint blind source separation by multiset canonical correlation analysis," *IEEE Trans. Signal Process.*, vol. 57, no. 10, pp. 3918–3929, Oct. 2009.

[5] V. D. Calhoun, T. Adali, G. D. Pearlson, and J. J. Pekar, "A method for making group inferences from functional MRI data using independent component analysis," *Hum. Brain Mapping*, vol. 14, no. 3, pp. 140–151, 2001.

[6] J.-H. Lee, T.-W. Lee, F. A. Jolesz, and S.-S. Yoo, "Independent vector analysis (IVA): Multivariate approach for fMRI group study," *NeuroImage*, vol. 40, no. 1, pp. 86–109, 2008.

[7] J.-H. Lee, T.-W. Lee, F. A. Jolesz, and S.-S. Yoo, "Independent vector analysis (IVA) for group fMRI processing of subcortical area," *Int. J. Imag. Syst. Technol.*, vol. 18, no. 1, pp. 29–41, 2008.

[8] Y. Liang, J. Harris, S. M. Naqvi, G. Chen, and J. A. Chambers, "Independent vector analysis with a generalized multivariate Gaussian source prior for frequency domain blind source separation," *Signal Process.*, vol. 105, pp. 175–184, Dec. 2014.

[9] Y. Li, W. Wang, T. Adali, and V. D. Calhoun, "CCA for joint blind source separation of multiple datasets with application to group FMRI analysis," in *Proc. Int. Conf. Acoust., Speech, Signal Process. (ICASSP)*, Las Vegas, NV, USA, Mar./Apr. 2008, pp. 1837–1840.

[10] N. M. Correa, T. Adali, Y.-O. Li, and V. D. Calhoun, "Canonical correlation analysis for data fusion and group inferences," *IEEE Signal Process. Mag.*, vol. 27, no. 4, pp. 39–50, Jun. 2010.

[11] X.-L. Li, T. Adalı, and M. Anderson, "Joint blind source separation by generalized joint diagonalization of cumulant matrices," *Signal Process.*, vol. 91, no. 10, pp. 2314–2322, Oct. 2011.

[12] X. Gong, Q. Lin, and K. Wang, "Joint non-orthogonal joint diagonalization based on LU decomposition and Jacobi scheme," in *Proc. ChinaSIP*, Beijing, China, Jul. 2013, pp. 25–29.

[13] X. Gong, X. Wang, and Q. Lin, "Generalized non-orthogonal joint diagonalization with LU decomposition and successive rotations," *IEEE Trans. Signal Process.*, vol. 63, no. 5, pp. 1322–1334, Mar. 2015.

[14] T. Kim, T. Eltoft, and T.-W. Lee, "Independent vector analysis: An extension of ICA to multivariate components," in *Proc. ICA*, Charleston, NC, USA, Mar. 2006, pp. 165–172.

[15] Y.-O. Li, T. Adali, and V. D. Calhoun, "Estimating the number of independent components for functional magnetic resonance imaging data," *Human Brain Mapping*, vol. 28, no. 11, pp. 1251–1266, 2007.

[16] X. Xu, Q. Wu, S. Wang, J. Liu, J. Sun, and A. Cichocki, "Whole brain fMRI pattern analysis based on tensor neural network," *IEEE Access*, vol. 6, pp. 29297–29305, 2018.

[17] F. Esposito and R. Goebel, "Extracting functional networks with spatial independent component analysis: The role of dimensionality, reliability and aggregation scheme," *Current Opinion Neurol.*, vol. 24, no. 4, pp. 378–385, Aug. 2011.

[18] B. Feng, Z. L. Yu, Z. Gu, and Y. Li, "Analysis of fMRI data based on sparsity of source components in signal dictionary," *Neurocomputing*, vol. 156, pp. 86–95, May 2015.

[19] M. Hui, R. Li, K. Chen, Z. Jin, L. Yao, and Z. Long, "Improved estimation of the number of independent components for functional magnetic resonance data by a whitening filter," *IEEE J. Biomed. Health Inform.*, vol. 17, no. 3, pp. 629–641, May 2013.

[20] A. Abou-Elseoud, T. Starck, J. Remes, J. Nikkinen, O. Tervonen, and V. Kiviniemi, "The effect of model order selection in group PICA," *Hum. Brain Mapping*, vol. 31, no. 8, pp. 1207–1216, 2010.
[21] A. A. Elseoud, H. Littow, J. Remes, T. Starck, J. Nikkinen, J. Nissilä, M. Timonen, O. Tervonen, and V. Kiviniemi, "Group-ICA model order highlights patterns of functional brain connectivity," *Frontiers Syst. Neurosci.*, vol. 5, p. 37, Jun. 2011.
[22] J. Qiao, S. Weng, P. Wang, J. Long, and Z. Wang, "Normalization of intrinsic neural circuits governing Tourette's Syndrome using cranial electrotherapy stimulation," *IEEE Trans. Biomed. Eng.*, vol. 62, no. 5, pp. 1272–1280, May 2015.
[23] J. Särelä and R. Vigário, "Overlearning in marginal distribution-based ICA: Analysis and solutions," *J. Mach. Learn. Res.*, vol. 4, pp. 1447–1469, Dec. 2003.
[24] C. F. Beckmann and S. M. Smith, "Probabilistic independent component analysis for functional magnetic resonance imaging," *IEEE Trans. Med. Imag.*, vol. 23, no. 2, pp. 137–152, Feb. 2004.
[25] L. Ma, B. Wang, X. Chen, and J. Xiong, "Detecting functional connectivity in the resting brain: A comparison between ICA and CCA," *Magn. Reson. Imag.*, vol. 25, no. 1, pp. 47–56, Jan. 2007.
[26] H. Akaike, "Information theory and an extension of the maximum likelihood principle," in *Selected Papers of Hirotugu Akaike*. New York, NY, USA: Springer, 1998, pp. 199–213.
[27] J. Rissanen, "Modeling by shortest data description," *Automatica*, vol. 14, no. 5, pp. 465–471, 1978.
[28] G. Schwarz, "Estimating the dimension of a model," *Ann. Statist.*, vol. 6, no. 2, pp. 461–464, 1978.
[29] J. E. Cavanaugh, "A large-sample model selection criterion based on Kullback's symmetric divergence," *Statist. Probab. Lett.*, vol. 42, no. 4, pp. 333–343, May 1999.
[30] Y.-O. Li, T. Adali, and V. D. Calhoun, "Sample dependence correction for order selection in fMRI analysis," in *Proc. 3rd IEEE Int. Symp. Biomed. Imag., Nano to Macro*, Apr. 2006, pp. 1072–1075.
[31] L. Yuan, X. Wei, H. Shen, L.-L. Zeng, and D. Hu, "Multi-center brain imaging classification using a novel 3D CNN approach," *IEEE Access*, vol. 6, pp. 49925–49934, 2018.
[32] M. Li, M. Li, Y. Liu, F. Chen, and D. Hu, "Including signal intensity increases the performance of blind source separation on brain imaging data," *IEEE Trans. Med. Imag.*, vol. 34, no. 2, pp. 551–563, Feb. 2015.
[33] A. Hyvärinen, *Independent Component Analysis*. New York, NY, USA: Wiley, 2001.
[34] X. Wu, L.-L. Zeng, H. Shen, M. Li, Y.-A. Hu, and D. Hu, "Blind source separation of functional MRI scans of the human brain based on canonical correlation analysis," *Neurocomputing*, vol. 269, pp. 220–225, Dec. 2017.
[35] G. Chen, F. Wang, J. C. Gore, and A. W. Roe, "Layer-specific BOLD activation in awake monkey V1 revealed by ultra-high spatial resolution functional magnetic resonance imaging," *NeuroImage*, vol. 64, pp. 147–155, Jan. 2013.
[36] Y. Xu, H. Yang, J. Li, J. Liu, and N. Xiong, "An effective dictionary learning algorithm based on fMRI data for mobile medical disease analysis," *IEEE Access*, vol. 7, pp. 3958–3966, 2019.
[37] K. Ugurbil *et al.*, "Pushing spatial and temporal resolution for functional and diffusion MRI in the human connectome project," *Neuroimage*, vol. 80, pp. 80–104, Oct. 2013.
[38] D. M. Barch *et al.*, "Function in the human connectome: Task-fMRI and individual differences in behavior," *Neuroimage*, vol. 80, pp. 169–189, Oct. 2013.
[39] M. F. Glasser, S. N. Sotiropoulos, J. A. Wilson, T. S. Coalson, B. Fischl, J. L. Andersson, J. Xu, S. Jbabdi, M. Webster, J. R. Polimeni, D. C. Van Essen, and M. Jenkinson, "The minimal preprocessing pipelines for the Human connectome project," *Neuroimage*, vol. 80, pp. 105–124, Oct. 2013.
[40] M. J. Jafri, G. D. Pearlson, M. Stevens, and V. D. Calhoun, "A method for functional network connectivity among spatially independent resting-state components in schizophrenia," *Neuroimage*, vol. 39, no. 4, pp. 1666–1681, Feb. 2008.
[41] M. C. Stevens, K. A. Kiehl, G. Pearlson, and V. D. Calhoun, "Functional neural circuits for mental timekeeping," *Hum. Brain Mapping*, vol. 28, no. 5, pp. 394–408, May 2007.
[42] K. Woods and K. W. Bowyer, "Generating ROC curves for artificial neural networks," *IEEE Trans. Med. Imag.*, vol. 16, no. 3, pp. 329–337, Jun. 1997.
[43] L. Xu, Z. Yao, J. Li, C. Lv, H. Zhang, and B. Hu, "Sparse feature learning with label information for Alzheimer's Disease classification based on magnetic resonance imaging," *IEEE Access*, vol. 7, pp. 26157–26167, 2019.
[44] Y. Du, E. A. Allen, H. He, J. Sui, L. Wu, and V. D. Calhoun, "Artifact removal in the context of group ICA: A comparison of single-subject and group approaches," *Hum. Brain Mapping*, vol. 37, no. 3, pp. 1005–1025, 2016.

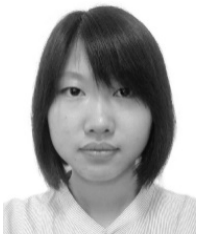

YAN ZHANG was born in Jilin, China, in 1994. She received the B.Sc. degree from the College of Intelligence Science and Technology, National University of Defense Technology (NUDT), Changsha, China, in 2017. Her research interests include blind source separation, neuroimaging analysis, and signal processing in functional magnetic resonance imaging (fMRI).

MING LI was born in Hebei, China, in 1978. He received the B.Sc. degree in automatic control from the Department of Automatic Control, National University of Defense Technology (NUDT), Changsha, China, in 2002, and the Ph.D. degree in control science and engineering from the College of Mechatronics and Automation (CMA), NUDT, in 2008, where he is currently an Associate Professor with the College of Intelligence Science and Technology. His research interests include spatiotemporal analysis on neuroimaging and signal processing in functional magnetic resonance imaging (fMRI).

HUI SHEN received the B.Sc. degree in automation and the Ph.D. degree in pattern recognition and intelligent system from the National University of Defense Technology (NUDT), Hunan, China, in 1997 and 2003, respectively. Since December 2003, he has been with NUDT. In 2013, he was a Visiting Scholar with Emory University, Atlanta, GA, USA. He was promoted as a Professor, in 2018. His research interests include cognitive neuroscience, image processing, and pattern recognition in neuroimaging.

LING-LI ZENG was born in Jiangxi, China, in 1984. He received the B.Sc., M.Sc. and Ph.D. degrees from the National University of Defense Technology (NUDT), China, in 2007, 2009, and 2014, respectively. From November 2012 to November 2013, he was a visiting Ph.D. student with the Harvard Medical School, Massachusetts General Hospital. Since 2014, he has been with NUDT, as a Lecturer and an Associate Professor. His research interests include cognitive neuroscience, image processing, and pattern recognition in neuroimaging.

DEWEN HU was born in Hunan, China, in 1963. He received the B.Sc. and M.Sc. degrees from Xi'an Jiaotong University, China, in 1983 and 1986, respectively, and the Ph.D. degree from the National University of Defense Technology (NUDT), in 1999. Since 1986, he has been with NUDT. From October 1995 to October 1996, he was a Visiting Scholar with the University of Sheffield, U.K. He was promoted as a Professor, in 1996. His research interests include image processing, system identification and control, neural networks, and cognitive science. He is an Action Editor of Neural Networks.